INFECTION AND IMMUNITY, Apr. 2011, p. 1512–1525 Vol. 79, No. 4
0019-9567/11/$12.00 doi:10.1128/IAI.01218-10


# The Cluster 1 Type VI Secretion System Is a Major Virulence Determinant in *Burkholderia pseudomallei*▽†

Mary N. Burtnick,[1] Paul J. Brett,[1] Sarah V. Harding,[2] Sarah A. Ngugi,[2] Wilson J. Ribot,[3] Narisara Chantratita,[4] Angelo Scorpio,[5] Timothy S. Milne,[2] Rachel E. Dean,[2] David L. Fritz,[3] Sharon J. Peacock,[6] Joanne L. Prior,[2] Timothy P. Atkins,[2] and David DeShazer[3]*

*Department of Microbiology and Immunology, University of South Alabama, Mobile, Alabama 36688[1]; Department of Biomedical Sciences, Defence Science and Technology Laboratory, Porton Down, Salisbury SP4 0JQ, United Kingdom[2]; Bacteriology Division, United States Army Medical Research Institute of Infectious Diseases, Fort Detrick, Frederick, Maryland 21702[3]; Department of Microbiology and Immunology and Mahidol-Oxford Tropical Medicine Research Unit, Faculty of Tropical Medicine, Mahidol University, Bangkok, Thailand[4]; National Biodefense Analysis and Countermeasures Center, Frederick, Maryland 21702[5]; and Department of Medicine, University of Cambridge, Addenbrooke's Hospital, Cambridge, United Kingdom[6]*

Received 16 November 2010/Returned for modification 11 December 2010/Accepted 27 January 2011

**The *Burkholderia pseudomallei* K96243 genome encodes six type VI secretion systems (T6SSs), but little is known about the role of these systems in the biology of *B. pseudomallei*. In this study, we purified recombinant Hcp proteins from each T6SS and tested them as vaccine candidates in the BALB/c mouse model of melioidosis. Recombinant Hcp2 protected 80% of mice against a lethal challenge with K96243, while recombinant Hcp1, Hcp3, and Hcp6 protected 50% of mice against challenge. Hcp6 was the only Hcp constitutively produced by *B. pseudomallei in vitro*; however, it was not exported to the extracellular milieu. Hcp1, on the other hand, was produced and exported *in vitro* when the VirAG two-component regulatory system was overexpressed in *trans*. We also constructed six *hcp* deletion mutants (Δ*hcp1* through Δ*hcp6*) and tested them for virulence in the Syrian hamster model of infection. The 50% lethal doses ($LD_{50}$s) for the Δ*hcp2* through Δ*hcp6* mutants were indistinguishable from K96243 (<10 bacteria), but the $LD_{50}$ for the Δ*hcp1* mutant was >$10^3$ bacteria. The *hcp1* deletion mutant also exhibited a growth defect in RAW 264.7 macrophages and was unable to form multinucleated giant cells in this cell line. Unlike K96243, the Δ*hcp1* mutant was only weakly cytotoxic to RAW 264.7 macrophages 18 h after infection. The results suggest that the cluster 1 T6SS is essential for virulence and plays an important role in the intracellular lifestyle of *B. pseudomallei*.**

Melioidosis, an infection of humans and animals, is caused by the Gram-negative bacterium *Burkholderia pseudomallei* (32, 36). The disease occurs primarily in tropical regions, especially Southeast Asia and northern Australia, where the etiologic agent is present in soil and water. The outcome of a *B. pseudomallei* infection can vary from asymptomatic seroconversion to fulminant septicemic melioidosis and death. Acute or chronic infection of any organ can occur, and lesions can form on any tissue but are most commonly found in the lungs, liver, spleen, lymph nodes, skin and soft tissues, and urinary tract. Latent infections can also occur, in which the organism remains dormant for as many as 62 years before recrudescence into an active infection (23). *B. pseudomallei* poses a significant threat to human and animal health, and there are legitimate concerns that it could be misused as a bioterrorism agent (12, 37).

Pathogenic bacteria export toxins and effector molecules by using macromolecular protein complexes known as secretion systems. A new secretion system, referred to as the type VI secretion system (T6SS), was recently described in Gram-negative bacteria (4). The T6SS apparatus structurally resembles an inverted bacteriophage tail, and it likely functions by injecting effector proteins directly into the cytosol of eukaryotic and/or bacterial cells (18). The *B. pseudomallei* K96243 genome encodes six T6SS gene clusters (28, 29), and it is currently unclear if these pathways are functionally redundant or are required for a specific niche or activity (5). Four of these T6SS gene clusters are also present in *B. mallei*, a virulent host-adapted clone of *B. pseudomallei* that causes glanders (38). In the initial description of T6SSs in *Burkholderia* by Schell et al. (28), the six *B. pseudomallei* K96243 gene clusters were designated T6SS-1 (BPSS1496 to BPSS1511), T6SS-2 (BPSS0515 to BPSS0533), T6SS-3 (BPSS2090 to BPSS2109), T6SS-4 (BPSS0166 to BPSS0185), T6SS-5 (BPSS0091 to BPSS0117), and T6SS-6 (BPSL3096 to BPSL3111). A subsequent publication by Shalom et al. (29) assigned the names *tss-5*, *tss-4*, *tss-6*, *tss-3*, *tss-2*, and *tss-1*, respectively, to these same gene clusters. Throughout this work we have used the Schell et al. nomenclature for these gene clusters.

The *B. mallei* T6SS gene cluster 1 (T6SS-1; BMAA0744 to BMAA0730) is important for actin-based motility, multinucleated giant cell (MNGC) formation, intracellular growth in murine macrophages, and virulence in hamsters (8, 28). In addition, we recently demonstrated that *B. mallei* T6SS-1 was expressed inside phagocytic vacuoles following uptake by murine macrophages (8). T6SS-1 was transcribed poorly when

* Corresponding author. Mailing address: Bacteriology Division, USAMRIID, 1425 Porter St., Fort Detrick, Frederick, MD 21702-5011. Phone: (301) 619-4871. Fax: (301) 619-8153. E-mail: david.deshazer@us.army.mil.

▽ Published ahead of print on 7 February 2011.

† The authors have paid a fee to allow immediate free access to this article.

bacteria were grown in rich medium, but it was induced as much as 30-fold when the *virAG* two-component regulatory system was overexpressed in *trans*. While the mechanism of action of the T6SS-1 effector(s) is unknown, the data support a model in which *B. mallei* T6SS-1 is active within phagocytic vacuoles and the secreted effector(s) is translocated into the host cell cytosol (11). Interestingly, *Vibrio cholerae* T6SS effectors are translocated into the cytosol of host cells in a process that requires trafficking of bacterial cells into an endocytic compartment (21).

Shalom et al. found that the *B. pseudomallei* T6SS-1 gene cluster was induced inside murine macrophages based on findings from *in vivo* expression technology (IVET) (29). The T6SS-1 genes were expressed poorly in cell culture medium alone but were induced ~12-fold when cocultured with macrophages. Interestingly, T6SS-1 played no role in the survival or growth of *B. pseudomallei* inside macrophages. Pilatz et al. demonstrated that a *B. pseudomallei* BPSS1509 transposon mutant exhibited a reduced ability to form plaques on PtK2 epithelial cell monolayers, indicating a defect in cell-to-cell spread (24). Furthermore, this mutant was highly attenuated in mice and yielded reduced bacterial burdens in the spleen, liver, and lung at 48 h postinfection. It is important to emphasize that neither study demonstrated that *B. pseudomallei* T6SS-1 is a functional secretion system.

Hcp proteins are integral surface-associated components of the T6SS apparatus that are commonly found in the supernatants of bacteria that express functional T6SSs. In this study, we assessed the role of six *B. pseudomallei* recombinant Hcp proteins as vaccine candidates in BALB/c mice and examined the reactivity of each protein with human melioidosis sera. The *in vitro* expression of *hcp1* through *-6* was assessed using RNA sequencing technology, and the *in vitro* production and export of Hcp1 through -6 was determined by immunoblotting with polyclonal mouse antisera. We also constructed deletion mutations in each *hcp* gene, examined the relative virulence of each mutant in the Syrian hamster model of acute melioidosis, and studied the intracellular behavior of the Δ*hcp1* mutant in murine macrophages. Taken together, the results suggest that the T6SS-1 is a critical *B. pseudomallei* virulence determinant that plays an important role in the intracellular lifestyle of the melioidosis pathogen.

## MATERIALS AND METHODS

**Bacterial strains, plasmids, and growth conditions.** The bacterial strains and plasmids used in this study are described in Table 1. *Escherichia coli* and *B. pseudomallei* were grown at 37°C on LB agar (Lennox L agar) or in LB broth (Lennox L broth). When appropriate, antibiotics were added at the following concentrations: 100 μg of ampicillin (Ap), 50 μg of carbenicillin (Cb), 15 μg of gentamicin (Gm), 25 μg of streptomycin (Sm), 25 μg of kanamycin (Km), 50 μg trimethoprim (Tp), and 25 μg of zeocin (Zeo) per ml for *E. coli* and 25 μg of polymyxin B (Pm), 25 μg of Gm, 25 μg of Km, and 25 μg of Sm per ml for *B. pseudomallei*. When $Km^r$ plasmids were conjugated to *B. pseudomallei* K96243, 500 μg/ml Km selection was employed. For induction studies, isopropyl-beta-D-thiogalactopyranoside (IPTG) was added to a final concentration of 0.5 mM. A 20-mg/ml stock solution of the chromogenic indicator 5-bromo-4-chloro-3-indolyl-β-D-galactoside (X-Gal) was prepared in *N*,*N*-dimethylformamide, and 40 μl was spread onto the surface of plate medium for blue/white screening in *E. coli* TOP10 (Invitrogen, Carlsbad, CA). All manipulations with *B. pseudomallei* were carried out in class II and class III microbiological safety cabinets located in designated biosafety level 3 (BSL-3) laboratories.

**DNA manipulation and plasmid conjugations.** Restriction enzymes, shrimp alkaline phosphatase, Antarctic phosphatase, and T4 DNA ligase were purchased from Roche Molecular Biochemicals and were used according to the manufacturer's instructions. When necessary, the End-It DNA end repair kit (Epicentre) was used to convert 5′ or 3′ protruding ends to blunt-ended DNA. DNA fragments used in cloning procedures were excised from agarose gels and purified with a GeneClean III kit (Qbiogene). Bacterial genomic DNA was prepared by using a previously described protocol (40). Plasmids were purified from overnight cultures by using Wizard Plus SV minipreps (Promega).

**PCR amplifications.** PCR primers are shown in Table 2. PCR products were sized and isolated using agarose gel electrophoresis, cloned using the pCR2.1-TOPO TA cloning kit (Invitrogen), and transformed into chemically competent *E. coli* TOP10. PCR amplifications were performed in a final reaction volume of 100 μl containing 1× *Taq* PCR master mix (Qiagen), 1 μM PCR primers, and approximately 200 ng of genomic DNA. PCR cycling was performed using a PTC-150 minicycler with a Hot Bonnet accessory (MJ Research, Inc.) and heated to 97°C for 5 min. This was followed by 30 cycles of a three-temperature cycling protocol (97°C for 30 s, 55°C for 30 s, and 72°C for 1 min) and one cycle at 72°C for 10 min. For PCR products greater than 1 kb, an additional 1 min per kb was added to the extension time. To generate blunt-ended PCR products, the 1× *Taq* PCR master mix was replaced with Vent DNA polymerase (New England BioLabs) and 1× FailSafe PreMix D (Epicentre).

**Construction of *B. pseudomallei* mutants.** The goal of this study was to assess the role of *B. pseudomallei* K96243 T6SS clusters in Hcp production and export, intracellular macrophage replication and survival, and hamster virulence. To accomplish this, we constructed mutants with in-frame *hcp* deletion mutations in each of the six T6SS gene clusters. Hcp is an integral component of the T6SS apparatus, and inactivation of *hcp* should render the targeted secretion apparatus nonfunctional (4, 26). Gene replacement experiments with *B. pseudomallei* were performed using the *sacB*-based vectors pMo130ΔNX and pEx18Km, as previously described (14, 20). Each deletion mutation was constructed by fusing PCR products immediately flanking the deleted region using splicing by overlapping extension-PCR (SOE-PCR), and the resulting products were cloned into pMo130ΔNX or pEx18Km. Briefly, the 3′ primer sequence for the upstream PCR product was designed to overlap the 3′ primer sequence for the downstream PCR product. The upstream and downstream PCR products were mixed and reamplified using the outer primers, resulting in the production of a fused product lacking the internal portion of the targeted gene. Recombinant derivatives of pMo130ΔNX and pEx18Km (Table 1) were electroporated into *E. coli* S17-1 (12.25 kV/cm) and conjugated with *B. pseudomallei* for 8 h, as described elsewhere (9, 34). Pm was used to counterselect *E. coli* S17-1. Optimal conditions for resolution of the *sacB* constructs were found to be LB agar lacking NaCl and containing 10% (wt/vol) sucrose, with incubation at 25°C for 3 to 4 days. Mutations were constructed in *B. pseudomallei* AI, a strain that is aminoglycoside sensitive due to a mutation in the *amrA* gene (Table 1). For *B. pseudomallei* mutant strains used in animal studies, the *amrA* mutation was repaired using pMo130-*amrA* (Table 1) in an attempt to make them as isogenic to K96243 as possible. *B. pseudomallei* deletion mutants were identified by PCR using the outer primers designed for SOE-PCR. As expected, the PCR products generated from the mutant strains were smaller than those obtained from the wild-type strain, and all were cloned and sequenced to confirm the mutations. The mutants generated in this study did not display any noticeable growth phenotype in LB broth or on LB agar (data not shown).

**Cloning, expression, and purification of V5-tagged Hcp proteins.** The *B. pseudomallei* K96243 *hcp* genes (*hcp1* [BPSS1498], *hcp2* [BPSS0518], *hcp3* [BPSS2098], *hcp4* [BPSS0171], *hcp5* [BPSS0099], and *hcp6* [BPSL3105]) were PCR amplified with the primers listed in Table 2, and the PCR products were cloned into pCRT7/CT-TOPO (Table 1). The resulting plasmids contained the *hcp* genes fused to a C-terminal V5 epitope and a polyhistidine (6×His) tag. The plasmids were transformed into *E. coli* BL21(DE3) and grown for 18 h in 250-ml disposable Erlenmeyer flasks containing 100 ml of LB with Zeo. Five milliliters of saturated culture was used to inoculate 400 ml of prewarmed LB with Zeo in a 1-liter disposable Erlenmeyer flask. A total of 2 liters of medium was inoculated for each strain. After 2 h of growth, 0.5 mM IPTG was added and the cultures were incubated an additional 4 h. The cultures were then centrifuged, and the cell pellets were resuspended in phosphate-buffered saline (PBS) containing DNase I and an EDTA-free protease inhibitor tablet (Roche). This cell paste was sonicated and centrifuged, and the resulting supernatant was filter sterilized (0.2 μm). Recombinant Hcp proteins were purified from the clarified supernatants using the GE Healthcare $AKTA_{FPLC}$ fast protein liquid chromatography system with 1-ml HisTrap HP affinity columns. His-tagged proteins were eluted from the affinity columns by applying a gradient of imidazole (50 mM to 500 mM). Fractions were collected, and aliquots were loaded into PhastGels, subjected to electrophoresis using the PhastSystem (GE Healthcare), and stained with PhastGel Blue R stain. Those fractions containing purified recombinant Hcp proteins

TABLE 1. Strains and plasmids used in this study

| Strain or plasmid | Relevant characteristics[a] | Source or reference |
|---|---|---|
| *E. coli* strains | | |
| TOP10 | General cloning and blue/white screening | Invitrogen |
| BL21(DE3) | *E. coli* B with DE3, a λ prophage carrying the T7 RNA polymerase gene | Novagen |
| S17-1 | Mobilizing strain with transfer genes of RP4 integrated on chromosome; $Sm^r$ $Tp^r$ $Pm^s$ | 31 |
| *B. pseudomallei* strains | | |
| K96243 | Clinical isolate from northeastern Thailand; $Gm^r$ $Sm^r$ $Km^r$ $Pm^r$ | 17 |
| AI | K96243 derivative harboring an 873-bp *amrA* deletion mutation (Δ*amrA*); $Gm^s$ $Sm^s$ $Km^s$ $Pm^r$ | S. Harding |
| AI2 | AI derivative with the Δ*amrA* mutation repaired; $Gm^r$ $Sm^r$ $Km^r$ $Pm^r$ | This study |
| DDS1498 | AI derivative harboring a 162-bp in-frame deletion mutation in *hcp1* (Δ*hcp1*); $Gm^s$ $Sm^s$ $Km^s$ $Pm^r$ | This study |
| DDS1498A | DDS1498 derivative with the Δ*amrA* mutation repaired; $Gm^r$ $Sm^r$ $Km^r$ $Pm^r$ | This study |
| DDS0518 | AI derivative harboring a 303-bp in-frame deletion mutation in *hcp2* (Δ*hcp2*); $Gm^s$ $Sm^s$ $Km^s$ $Pm^r$ | This study |
| DDS0518A | DDS0518 derivative with the Δ*amrA* mutation repaired; $Gm^r$ $Sm^r$ $Km^r$ $Pm^r$ | This study |
| DDS2098 | AI derivative harboring a 186-bp in-frame deletion mutation in *hcp3* (Δ*hcp3*); $Gm^s$ $Sm^s$ $Km^s$ $Pm^r$ | This study |
| DDS2098A | DDS2098 derivative with the Δ*amrA* mutation repaired; $Gm^r$ $Sm^r$ $Km^r$ $Pm^r$ | This study |
| DDS0171 | AI derivative harboring a 321-bp in-frame deletion mutation in *hcp4* (Δ*hcp4*); $Gm^s$ $Sm^s$ $Km^s$ $Pm^r$ | This study |
| DDS0171A | DDS0171 derivative with the Δ*amrA* mutation repaired; $Gm^r$ $Sm^r$ $Km^r$ $Pm^r$ | This study |
| DDS0099 | AI derivative harboring a 192-bp in-frame deletion mutation in *hcp5* (Δ*hcp5*); $Gm^s$ $Sm^s$ $Km^s$ $Pm^r$ | This study |
| DDS0099A | DDS0099 derivative with the Δ*amrA* mutation repaired; $Gm^r$ $Sm^r$ $Km^r$ $Pm^r$ | This study |
| DDL3105 | AI derivative harboring a 216-bp in-frame deletion mutation in *hcp6* (Δ*hcp6*); $Gm^s$ $Sm^s$ $Km^s$ $Pm^r$ | This study |
| DDL3105A | DDL3105 derivative with the Δ*amrA* mutation repaired; $Gm^r$ $Sm^r$ $Km^r$ $Pm^r$ | This study |
| DDS1503-1 | AI derivative harboring a deletion of the 743-bp StuI fragment at the 5′ end of *vgrG1* ($\Delta vgrG1_{561\text{-}1303}$); $Gm^s$ $Sm^s$ $Km^s$ $Pm^r$ | This study |
| DDS1503-1A | DDS1503-1 derivative with the Δ*amrA* mutation repaired; $Gm^r$ $Sm^r$ $Km^r$ $Pm^r$ | This study |
| DDS1503-2 | AI derivative harboring a deletion of the 894-bp PstI fragment at the 3′ end of *vgrG1* ($\Delta vgrG1_{1770\text{-}2663}$); $Gm^s$ $Sm^s$ $Km^s$ $Pm^r$ | This study |
| DDS1503-2A | DDS1503-2 derivative with the Δ*amrA* mutation repaired; $Gm^r$ $Sm^r$ $Km^r$ $Pm^r$ | This study |
| Plasmids | | |
| pCR2.1-TOPO | 3,931-bp TA vector; pMB1 *oriR*; $Km^r$ $Ap^r$ | Invitrogen |
| pCR2.1-BPSS1498 | pCR2.1-TOPO containing 1,396-bp PCR product generated with BPSS1498-1 and BPSS1498-4 | This study |
| pCR2.1-*amrA* | pCR2.1-TOPO containing 1,943-bp PCR product generated with amrR-1/amrB-1 | This study |
| pCR2.1-ΔBPSS1498 | pCR2.1-TOPO containing 1,252-bp fragment generated by joining BPSS1498-1/BPSS1498-2 and BPSS1498-3/BPSS1498-4 PCR products via SOE-PCR | This study |
| pCR2.1-ΔBPSS0518 | pCR2.1-TOPO containing 1,212-bp fragment generated by joining BPSS0518-1/BPSS0518-2 and BPSS0518-3/BPSS0518-4 PCR products via SOE-PCR | This study |
| pCR2.1-ΔBPSS2098 | pCR2.1-TOPO containing 1,325-bp fragment generated by joining BPSS2098-1/BPSS2098-2 and BPSS2098-3/BPSS2098-4 PCR products via SOE-PCR | This study |
| pCR2.1-ΔBPSS0171 | pCR2.1-TOPO containing 1,301-bp fragment generated by joining BPSS0171-1/BPSS0171-2 and BPSS0171-3/BPSS0171-4 PCR products via SOE-PCR | This study |
| pCR2.1-ΔBPSL3105 | pCR2.1-TOPO containing 1,250-bp fragment generated by joining BPSL3105-1/BPSL3105-2 and BPSL3105-3/BPSL3105-4 PCR products via SOE-PCR | This study |
| pCR2.1-BPSS1503 | pCR2.1-TOPO containing 3,048-bp PCR product generated with VgrG1-5′ and VgrG1-3′ | This study |
| pCR2.1-1503 | pCR2.1-TOPO containing 1,590-bp PCR product generated with 1503-up2 and 1503-dn2 | This study |
| pCR2.1-ΔA0737 | pCR2.1-TOPO containing deletion of 743-bp StuI fragment at the 5′ end of *vgrG1* ($\Delta vgrG1_{561\text{-}1303}$) | 30 |
| pCR4Blunt-TOPO | 3,956-bp positive selection cloning vector; pUC ori; $Km^r$ $Ap^r$ | Invitrogen |
| pCR4-ΔBPSS0099 | pCR4Blunt-TOPO containing 1,301-bp fragment generated by joining BPSS0099–/BPSS0099-2 and BPSS0099-3/BPSS0099-4 PCR products via SOE-PCR | This study |
| pCRT7/CT-TOPO | 2.7-kb TA vector; allows C-terminal fusions to V5 epitope and 6×His tag under the control of a T7 promoter; pMB1 *oriR*; $Ap^r$ $Zeo^r$ | Invitrogen |
| pCRT7/CT-BPSS1498 | pCRT7/CT-TOPO containing PCR product generated with 1498-up and 1498-dn | This study |
| pCRT7/CT-BPSS0518 | pCRT7/CT-TOPO containing PCR product generated with 0518-up and 0518-dn | This study |
| pCRT7/CT-BPSS2098 | pCRT7/CT-TOPO containing PCR product generated with 2098-up and 2098-dn | This study |
| pCRT7/CT-BPSS0171 | pCRT7/CT-TOPO containing PCR product generated with 0171-up and 0171-dn | This study |
| pCRT7/CT-BPSS0099 | pCRT7/CT-TOPO containing PCR product generated with 0099-up and 0099-dn | This study |
| pCRT7/CT-BPSL3105 | pCRT7/CT-TOPO containing PCR product generated with 3105-up and 3105-dn | This study |
| pMo130 | Suicide vector for allelic exchange in *Burkholderia*; ColE1 *ori* RK2 *oriT xylE sacB*; $Km^r$ | 14 |
| pMo130ΔNX | pMo130 digested with NotI and XbaI, blunt ended, and ligated to eliminate NotI, PstI, BamHI, and XbaI sites | This study |
| pMo130-ΔBPSS1498 | pMo130ΔNX containing NheI insert from pCR2.1-ΔBPSS1498 | This study |
| pMo130-ΔBPSS0518 | pMo130ΔNX containing NheI insert from pCR2.1-ΔBPSS0518 | This study |
| pMo130-ΔBPSS2098 | pMo130ΔNX containing NheI insert from pCR2.1-ΔBPSS2098 | This study |
| pMo130-ΔBPSS0171 | pMo130ΔNX containing NheI insert from pCR2.1-ΔBPSS0171 | This study |
| pMo130-ΔBPSL3105 | pMo130ΔNX containing NheI insert from pCR2.1-ΔBPSL3105 | This study |
| pMo130-ΔBPSS0099 | pMo130ΔNX containing NheI insert from pCR4-ΔBPSS0099 | This study |
| pMo130-1503 | pMo130ΔNX containing BamHI insert from pCR2.1-1503 cloned into the BglII site | This study |
| pMo130-ΔBPSS1503 | pMo130-1503 with 894-bp PstI fragment removed | This study |

*Continued on following page*

TABLE 1—*Continued*

| Strain or plasmid | Relevant characteristics[a] | Source or reference |
|---|---|---|
| pBHR2 | Broad-host-range vector; $Km^r$ | 28 |
| pBHR2-BPSS1498 | pBHR2 containing XbaI-SpeI insert from pCR2.1-BPSS1498 | This study |
| pBHR2-*virAG* | pBHR2 derivative containing *B. mallei virAG* genes | 28 |
| pBHR1-TG | Broad-host-range vector containing *gfp*; $Km^r$ | 8 |
| pBHR1TG-BPSS1503 | pBHR1-TG containing EcoRV insert from pCR2.1-BPSS1503 cloned into the ScaI site | This study |
| pEx18Km | pEx18Tc derivative containing the 1,003-bp $Km^r$ PCR product generated with nptF and nptR from pCR2.1-TOPO; $Km^r$ $Tc^s$ | 30 |
| pΔA0737 | pEx18Km derivative containing XbaI-SpeI fragment from pCR2.1-ΔA0737 in XbaI site | 30 |

[a] Tc, tetracycline.

were pooled and dialyzed against PBS overnight at 4°C. Hcp2 and Hcp5 were eluted and dialyzed in buffers containing 10% glycerol and 2.5% glucose, in an attempt to prevent protein precipitation. The purified Hcp proteins and protein standards were subjected to the colorimetric bicinchoninic acid assay, and the absorbances at 562 nm were determined using an Ultrospec 4000 spectrophotometer. The final concentrations of the Hcp protein solutions were determined by comparing the mean of two replicates against a standard slope generated using protein solutions of known concentrations.

**Immunoblot analysis of Hcp proteins with human serum samples.** Human sera were obtained from 10 patients with culture-proven melioidosis at Sappasithiprasong Hospital, Ubon Rachathani, Thailand. Eight of the patients had indirect hemagglutination (IHA) titers of 160 to 10,240, while two had titers of 0. Sera were also obtained from 10 blood donors from Ubon Rachathani who had no history of melioidosis. All normal donors had IHA titers of 0. Approximately 1 μg of each recombinant Hcp protein and a *B. pseudomallei* crude lysate were applied to 13% acrylamide gels, subjected to SDS-PAGE, and transferred to

TABLE 2. PCR primers used in this study

| Primer name | Sequence (5′–3′) | Target |
|---|---|---|
| 1498-up | ATGCTGGCCGGAATATATCTC | BPSS1498 |
| 1498-dn | GCCATTCGTCCAGTTTGCGG | BPSS1498 |
| 0518-up | ATGGCAAATGCTTTGGTTGA | BPSS0518 |
| 0518-dn | GATCGGCGCGTTCTGCTTCA | BPSS0518 |
| 2098-up | ATGGGCGTCGCAATGTTTATG | BPSS2098 |
| 2098-dn | CATCTCGGTGTTCTCCTTGATG | BPSS2098 |
| 0171-up | ATGGCGCAGGATATTTTTCTG | BPSS0171 |
| 0171-dn | GGCTTCCTTGTTGCCCTTGATG | BPSS0171 |
| 0099-up | ATGTCGCACGACATTTTCCTC | BPSS0099 |
| 0099-dn | CGCCGCGTTCTTCTTGATGTC | BPSS0099 |
| 3105-up | ATGTTACACATGCATTTGAAG | BPSS3105 |
| 3105-dn | GACCGCGTAGGTCTTGTCGTTC | BPSS3105 |
| BPSS1498-1 | GCTAGCATCCGCCAGTACGTCGTCGAC | BPSS1497 |
| BPSS1498-2 | GGATCCTTTAAATCTAGACGGCGACGATCTGTCCATTTC | BPSS1498 |
| BPSS1498-3 | TCTAGATTTAAAGGATCCCCGCACAAAGACGATAGCAAC | BPSS1498 |
| BPSS1498-4 | GCTAGCTCAGGAAATCGTTCGGATATC | BPSS1499 |
| BPSS0518-1 | GCTAGCATCTTCGCGACCTGCCGTTTC | BPSS0517 |
| BPSS0518-2 | GGATCCTTTAAATCTAGACTGCCAGCTCTGGATCTGGAT | BPSS0518 |
| BPSS0518-3 | TCTAGATTTAAAGGATCCACGGATCAGATCCGCATCAAC | BPSS0518 |
| BPSS0518-4 | GCTAGCATAACCACTCAGATAGTCGAG | BPSS0519 |
| BPSS2098-1 | GCTAGCCTCGCGAAGAACGGCTTCATG | BPSS2099 |
| BPSS2098-2 | GGATCCTTTAAATCTAGAGAACGACTGGATGTCGGTCCA | BPSS2098 |
| BPSS2098-3 | TCTAGATTTAAAGGATCCCAGATCGAGTTCATGCGCGTG | BPSS2098 |
| BPSS2098-4 | GCTAGCCTCGAACATCAGCACGTTGTG | BPSS2097 |
| BPSS0171-1 | GCTAGCGCCGAATACGACGATTCCGAC | BPSS0172 |
| BPSS0171-2 | GGATCCTTTAAATCTAGAGTGCATCGTCGATTCCTGCTG | BPSS0171 |
| BPSS0171-3 | TCTAGATTTAAAGGATCCGTCACGACGAGCTTCGACATC | BPSS0171 |
| BPSS0171-4 | GCTAGCCATTTTCCGGGTTCGGTGATC | BPSS0170 |
| BPSS0099-1 | GCTAGCCATCGAAAGAACACCGACTAC | BPSS0098 |
| BPSS0099-2 | GGATCCTTTAAATCTAGAGACCTCGATTTCGCCCTTGTG | BPSS0099 |
| BPSS0099-3 | TCTAGATTTAAAGGATCCCCGCTCGAATACATCAAGCTC | BPSS0099 |
| BPSS0099-4 | GCTAGCTTTCAGCTCGTACAGCCGCAC | BPSS0100 |
| BPSL3105-1 | GCTAGCCACTGCAAGAATTCCGATTAC | BPSL3106 |
| BPSL3105-2 | GGATCCTTTAAATCTAGACGGCTGAACGATCGAGTGATC | BPSL3105 |
| BPSL3105-3 | TCTAGATTTAAAGGATCCGAGATCAAGCTGAAGTACGTG | BPSL3105 |
| BPSL3105-4 | GCTAGCGACTGCTCGTTCAGCTCGAAC | BPSL3104 |
| amrR-1 | GCTAGCTCGGACAGGTCGAAGCCTTC | *amrR* |
| amrB-1 | GCTAGCACGATTTTCAGGCGGTTCTG | *amrB* |
| VgrG1-5′ | GATATCCAGGAGTTCCCGATGCCTTC | BPSS1503 |
| VgrG1-3′ | GATATCTCAGCCGAGCTGGATCAGTTG | BPSS1503 |
| 1503-up2 | GGATCCTCGTCGCACCGCAGCGTCGTC | BPSS1503 |
| 1503-dn2 | GGATCCTCAGCCGAGCTGGATCAGTTGGCC | BPSS1503 |

nitrocellulose membranes. The membranes were blocked with 5% skim milk in PBS for 30 min and reacted with pooled human serum samples diluted 1:2,000 in 3% skim milk in PBS containing 0.1% Tween 20 (PBST) for 2 h. The secondary antibody was a rabbit anti-human IgG horseradish peroxidase-labeled conjugate (Dako) that was diluted 1:2,000 in PBST and incubated for 1 h. The bands were developed by the use of $H_2O_2$ and 3,3′-diaminobenzidine (DAB; Sigma). The crude lysate was prepared by resuspending a loopful of *B. pseudomallei* K96243 grown on Ashdown agar (1) in 250 μl of SDS-PAGE 1× sample buffer. The suspension was boiled for 10 min, the supernatant was separated after centrifugation, and 3 μl was used for immunoblot analysis.

**Immunoblot analysis of Hcp proteins with polyclonal mouse antisera.** The methods followed for immunoblot analysis were described in detail previously (28). The membranes were incubated with a 1:15,000 dilution of polyclonal mouse anti-Hcp sera (pooled sera from six mice) and a 1:5,000 dilution of a peroxidase-labeled goat anti-mouse IgG (H+L) antibody (KPL) and developed with 3,3′-5,5′-tetramethylbenzidine membrane peroxidase substrate (KPL).

**RNA isolation, sequencing, and bioinformatics.** *B. pseudomallei* AI(pBHR2) and AI(pBHR2-*virAG*) were grown overnight in LB broth containing 25 μg/ml Km, and 250 μl was used to inoculate three 50-ml cultures (biological replicates) for each strain. Four biological replicates of K96243 were processed in a similar fashion. All cultures were grown for ~8 h to the mid-logarithmic phase of growth (optical density at 600 nm of 0.85), and total RNA was isolated from each culture by using TRIzol reagent (Invitrogen). After rRNA depletion, the RNA samples were sequenced using the SOLiD 3 and 4 platforms (Life Technologies Corp., Carlsbad, CA). Library preparations, fragment library protocols, and SOLiD sequencing were performed according to the manufacturer's instructions. The data generated were strand specific and derived from fragment read lengths of 50 bp in length. Samples were run through the SAET (SOLiD accuracy enhancement tool) program to increase the accuracy and the quality of reads.

For bioinformatics expression analysis, the samples were analyzed using the CLC genomics workbench RNA-Seq pipeline (CLC bio, Cambridge, MA). The maximum number of mismatches allowed was 2, and the maximum number of hits per read was 10. *B. pseudomallei* K96243 (accession numbers NC_006350 and NC_006351) was used as the reference genome. Expression values are given as reads per kilobase of coding sequence per million reads (RPKM). The RNA sequencing and expression measurements were performed by EdgeBio (Gaithersburg, MD).

**Statistical analysis of RNA sequencing studies.** RPKM comparisons among gene clusters and between individual genes in a given cluster were performed with the Wilcoxon rank sum test.

**BALB/c mouse vaccination and challenge studies.** Female BALB/c mice (six per group) were vaccinated by the intraperitoneal (i.p.) route with 10 μg of recombinant Hcp protein mixed with the Sigma adjuvant system (SAS) in a total volume of 100 μl. Three inoculations were given at 2-week intervals, and 3 weeks after the final boost serum was collected from the tail vein by venipuncture and pooled according to vaccination group. Five weeks after the final boost the animals were challenged i.p. with ~50,000 CFU of *B. pseudomallei* K96243. The animals were observed daily for 42 days, and the survivors were euthanized and their spleens were removed, homogenized in sterile PBS, serially diluted, and spread onto LB plates to determine if the animals were chronically colonized. These studies were conducted at Dstl Porton Down, United Kingdom.

**Hamster virulence studies.** Female Syrian hamsters (five per group) were infected by the i.p. route with a range of $10^0$ to $10^3$ CFU for each strain of *B. pseudomallei* examined. Mortality was recorded daily for 14 days, and on day 15 the surviving animals from each group were euthanized and the $LD_{50}$ was calculated (27).

Research was conducted in compliance with the Animal Welfare Act and other federal statutes and regulations relating to animals and experiments involving animals and adhered to principles stated in the Guide for the Care and Use of Laboratory Animals, National Research Council (22). The facility where this research was conducted, USAMRIID, is fully accredited by the Association for Assessment and Accreditation of Laboratory Animal Care International.

**Comparative histopathology of hamsters infected with the wild type and the Δ*hcp1* protein.** Groups of three hamsters were injected i.p. with ~8 CFU of wild-type and ~630 CFU of Δ*hcp1* protein and euthanized 2 days postinfection, and tissues were immersed in 10% neutral buffered formalin. Forty-eight hours postinfection was chosen as the end point because this is when the animals infected with the wild type became noticeably ill (death often occurred within 72 h of infection). A higher dose of Δ*hcp1* protein was used for the comparative histological analysis, due to its significantly higher $LD_{50}$ (see Table 6). Once properly fixed, tissue samples were routinely processed, embedded in paraffin, sectioned at 5 to 6 μm, mounted on glass microslides, and stained with hematoxylin and eosin (H&E). Stained tissue sections were evaluated under a light microscope.

**Cell culture and macrophage survival assays.** The RAW 264.7 cell line (ATCC TIB-71) was maintained in Dulbecco's modified Eagle's medium supplemented with 10% (vol/vol) heat-inactivated fetal bovine serum (DMEM-10; Invitrogen). For macrophage survival assays, RAW 264.7 cells were resuspended in DMEM-10, transferred into 24-well tissue culture plates at a density of $1 \times 10^6$ cells/well, and incubated overnight at 37°C under an atmosphere of 5% $CO_2$. Bacterial uptake and survival were measured in modified Km protection assays as previously described (6, 7). In brief, bacterial suspensions were added in triplicate to RAW 264.7 cells at a multiplicity of infection (MOI) of 1 to 2 and incubated for 1 h. Monolayers were then washed twice with Hanks' balanced salt solution (HBSS) and incubated with fresh DMEM-10 containing 250 μg/ml Km. Infected monolayers were lysed at 3, 6, 12, and 18 h postinfection with 0.2% (vol/vol) Triton X-100, and serial dilutions of the lysates were plated to enumerate bacterial loads. The data were plotted using GraphPad Prism 5 (GraphPad Software Inc., San Diego, CA). Statistical differences were determined using an unpaired Student *t* test with the significance set at $P < 0.05$. The error bars in Fig. 6 represent standard deviations (SD).

**Cytotoxicity assays.** Filter-sterilized *B. pseudomallei*-infected RAW 264.7 cell supernatants were assayed for lactate dehydrogenase (LDH) release by using a CytoTox 96 nonradioactive cytotoxicity assay kit (Promega). Maximum release was achieved by lysis of monolayers with Triton X-100 at a final concentration of 1% (vol/vol). The LDH released by uninfected cells was designated the spontaneous release. Cytotoxicity was calculated as follows: percent cytotoxicity = (test LDH release − spontaneous release)/(maximal release − spontaneous release). The data were plotted using GraphPad Prism 5 (GraphPad Software Inc., San Diego, CA). Statistical differences were determined using an unpaired Student *t* test with the significance set at $P < 0.05$. The error bars in Fig. 6 represent the SD.

**Immunofluorescence staining and microscopy.** RAW 264.7 cells (~$1 \times 10^5$ to $2 \times 10^5$ cells/well) were grown overnight on 12-mm glass coverslips in 24-well plates at 37°C under 5% $CO_2$. Cells were infected with green fluorescent protein (GFP)-expressing *B. pseudomallei* strains at an MOI of 4 to 5 as described for the macrophage survival assays. For aminoglycoside-resistant *B. pseudomallei* strains, imipenem at 10 μg/ml was used to suppress the growth of extracellular bacteria. Monolayers were immunostained at room temperature essentially as previously described (7, 8). Briefly, at 12 and 18 h postinfection, monolayers were fixed in 2.5% paraformaldehyde for 15 min, washed three times with PBS, and then permeabilized in PBS containing 10% normal goat serum (Invitrogen) and 0.1% (wt/vol) saponin (SS-PBS) for 20 min. Cells were incubated with Alexa Fluor 568 phalloidin (1:100; Invitrogen) and DRAQ5 (1:2,000; Alexis Biochemicals) in SS-PBS for 45 min. After three washes with PBS and two washes with water, coverslips were mounted on glass slides using Prolong Gold antifade reagent (Invitrogen). Fluorescence microscopy was performed with a Nikon 90i imaging system, and images were acquired using NIS-Elements software (Nikon).

## RESULTS

**Human melioidosis serum samples react with Hcp1.** To determine if Hcp proteins were produced during infection, we expressed and purified recombinant Hcp proteins and reacted them with human melioidosis serum samples. The recombinant *B. pseudomallei* Hcp proteins were between 20 and 25 kDa in size and contained little, if any, contaminating *E. coli* proteins (Fig. 1). We performed an immunoblot assay using pooled sera from 10 healthy individuals, and there was no reactivity with the Hcp proteins and only weak reactivity with a crude *B. pseudomallei* lysate (Fig. 2A). On the other hand, pooled sera from 10 culture-confirmed melioidosis cases from Thailand reacted strongly with Hcp1 and the crude *B. pseudomallei* lysate (Fig. 2B). We next tested each of the 10 sera individually, and 9 contained antibodies that reacted with Hcp1 (data not shown). Eight of the patients had IHA titers of 160 to 10,240, while two had titers of 0. Interestingly, the patient that did not react with Hcp1 also had an IHA titer of 0. The results suggest that Hcp1 is produced by *B. pseudomallei in vivo*

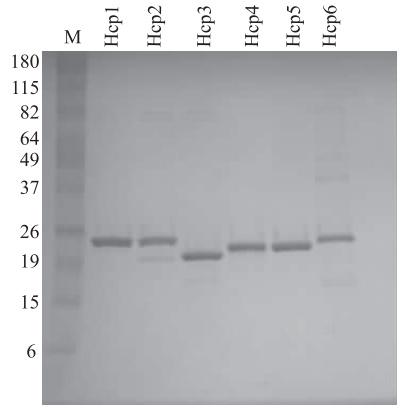


FIG. 1. SDS-PAGE of recombinant Hcp proteins encoded by six T6SS gene clusters in *B. pseudomallei* K96243. The recombinant Hcp proteins contain C-terminal 6×His tags and were purified by immobilized metal affinity chromatography. Approximately 1 μg of protein was subjected to SDS-PAGE and stained with colloidal Coomassie blue. The relative migrations of molecular mass protein standards (lane M; in kDa) are indicated on the left. The recombinant proteins are designated Hcp1 (BPSS1498), Hcp2 (BPSS0518), Hcp3 (BPSS2098), Hcp4 (BPSS0171), Hcp5 (BPSS0099), and Hcp6 (BPSL3105).

and is immunogenic but that Hcp2 through -6 are not produced or are not immunogenic during human infection. In addition, the results suggest that Hcp1 might be a good candidate for use as a serodiagnostic reagent for melioidosis.

**Hcp vaccination and challenge studies in BALB/c mice.** BALB/c mice were vaccinated with the recombinant Hcp proteins and challenged with a lethal dose of *B. pseudomallei* to determine if these proteins represented potential melioidosis vaccine candidates. Groups of six mice were vaccinated with a mixture of Hcp protein and SAS, a stable oil-in-water adjuvant. The mice were inoculated three times, and serum was collected from each mouse and pooled. Immunoblot assays performed with polyclonal Hcp antisera demonstrated that the mice produced a specific antibody response to each of the recombinant Hcp proteins (data not shown). The mice were challenged 5 weeks after the final i.p. boost with ~$5 \times 10^4$ CFU of *B. pseudomallei* K96243, a challenge dose that represents approximately 50 times the minimum lethal dose (MLD). The group that received no immunogen or adjuvant (naïve) all died by day 16, whereas the group that received SAS alone did not all perish until day 42. The delayed time to death in the SAS group suggests that it might be a relatively good adjuvant for use in *B. pseudomallei* challenge studies in BALB/c mice. Five of the six mice that were vaccinated with Hcp2 were still alive 6 weeks after challenge; however, all were chronically colonized (Table 3). The mice that were vaccinated with Hcp1, Hcp3, or Hcp6 exhibited 50% survival 42 days after challenge (Table 3). Interestingly, *B. pseudomallei* did not colonize the spleens of two surviving Hcp1-vaccinated animals or any of the surviving Hcp6-vaccinated animals. Only two of the Hcp4-vaccinated mice, and none of the Hcp5-vaccinated mice, were alive at the end of the experiment (Table 3).

We repeated the vaccination experiment with the most promising candidates, Hcp1, Hcp2, Hcp3, and Hcp6, using more animals in each group and a similar challenge dose.

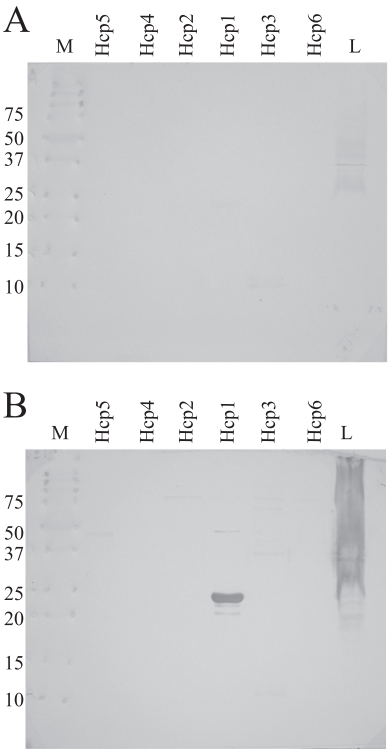


FIG. 2. Immunoblot analysis of *B. pseudomallei* recombinant Hcp proteins with human serum samples. A crude *B. pseudomallei* lysate (L) and the recombinant Hcp proteins were separated by SDS-PAGE, transferred to nitrocellulose membranes, and incubated with pooled sera from 10 healthy donors (A) or pooled sera from 10 melioidosis patients (B). The relative migrations of molecular mass protein standards (lanes M; in kDa) are indicated on the left. The recombinant Hcp proteins are as described in the legend for Fig. 1.

While all 12 of the naïve animals perished by day 15, there were still 2/12 survivors in the SAS-only control group on day 42. The Hcp1, Hcp2, Hcp3, and Hcp6 groups contained 2/11, 1/12, 3/11, and 4/12 survivors on day 42, respectively. In com-

TABLE 3. Results of vaccination of BALB/c mice with recombinant Hcp proteins and challenge with 50 MLD of *B. pseudomallei* K96243

| Antigen[a] | No. of survivors/ total vaccinated | Bacteria present in the spleens of surviving animals[b] | | | | |
|---|---|---|---|---|---|---|
| | | Animal 1 | Animal 2 | Animal 3 | Animal 4 | Animal 5 |
| Hcp1 | 3/6 | $10^3$ | 0 | 0 | NA[c] | NA |
| Hcp2 | 5/6 | $>10^5$ | $>10^5$ | $10^2$ | $10^2$ | $10^2$ |
| Hcp3 | 3/6 | $10^2$ | $10^3$ | $10^3$ | NA | NA |
| Hcp4 | 2/6 | $10^3$ | $10^3$ | NA | NA | NA |
| Hcp5 | 0/5 | NA | NA | NA | NA | NA |
| Hcp6 | 3/6 | 0 | 0 | 0 | NA | NA |
| Naïve | 0/6 | NA | NA | NA | NA | NA |
| SAS only | 0/6 | NA | NA | NA | NA | NA |

[a] Recombinant Hcp proteins were mixed with SAS and delivered parentally three times over the course of a month. One mouse in the Hcp5 group died during vaccination, and so in that group only five animals were challenged with K96243.

[b] Spleens were removed from euthanized animals on day 42 and immersed in 1 ml of PBS and homogenized, and 100-μl aliquots were plated to estimate the total number of bacteria present.

[c] NA, not applicable.

TABLE 4. Expression profiling of *B. pseudomallei* K96243 T6SS clusters in LB broth

| T6SS cluster | Mean RPKM[a] | RPKM range | Ratio (mean RPKM)/*narK* |
|---|---|---|---|
| 1 | 0.4 | 0.0–6.1 | 0.06 |
| 2 | 2.3 | 0.07–24 | 0.4 |
| 3 | 0.2 | 0.0–1.0 | 0.03 |
| 4 | 0.9 | 0.2–6.1 | 0.2 |
| 5 | 0.7 | 0.08–5.9 | 0.1 |
| 6 | 47.1[b] | 2.2–264 | 7.5[b] |

[a] Values are the mean number of reads per kilobase of coding sequence per million reads for each cluster from four biological replicates.
[b] *P* values were <0.001 for all comparisons between T6SS cluster 6 and T6SS clusters 1 through 5.

parison with the first experiment, the percent survival on day 42 was lower in the repeat experiment for all of the Hcps (Hcp1, 50% versus 18%; Hcp2, 80% versus 8%; Hcp3, 50% versus 27%; Hcp6, 50% versus 33%). While the challenge doses for the experiments were relatively stringent, the data suggest that, individually, the Hcp proteins would probably not serve as good melioidosis vaccine candidates because of their poor protection against morbidity and mortality and their inability to prevent chronic colonization after challenge.

**Expression profiling of the *B. pseudomallei* T6SS gene clusters in LB broth.** T6SS gene clusters are often tightly regulated at the transcriptional and/or posttranslational level, and the environmental signal(s) required for their expression or production is often not known (2). We utilized SOLiD RNA sequencing to analyze the expression of the *B. pseudomallei* K96243 T6SS gene clusters in LB broth. The RPKM values were derived from four biological replicates, and their average quality value (QV) was 19.3. It was observed that the T6SS-6 genes were expressed on average >100-fold higher than the genes in T6SS clusters 1 through 5 ($P < 0.001$, Wilcoxon rank sum test). The overall mean RPKM value for T6SS-6 was 47.1, with a range of 2.2 to 264 (Table 4). As a ratio to the housekeeping gene *narK* (13), the mean RPKM expression values of the genes composing T6SS clusters 1 through 5 were all found to be less than 1. In comparison, the genes composing the T6SS-6 cluster exhibited a ratio of 7.5 (Table 4). These results clearly demonstrate that the T6SS-6 gene cluster was transcribed at a relatively high level in LB broth but that the other T6SS gene clusters were expressed poorly in this medium.

**Hcp6 is produced *in vitro* but is not exported.** Hcp proteins are integral extracellular components of the T6SS apparatus and are commonly found in the supernatant of bacteria that express functional T6SSs (4). We performed immunoblot assays with Hcp-specific antisera and found that Hcp1 through Hcp5 were not produced or exported when *B. pseudomallei* was grown in LB broth (data not shown). This result was not unexpected, as the T6SS gene clusters 1 through 5 were expressed poorly in LB broth (Table 4).

T6SS-6 was highly expressed in LB broth, and we wanted to determine if Hcp6 was produced and/or exported using this medium. We grew *B. pseudomallei* wild type and the Δ*hcp6* mutant to mid-logarithmic phase and performed an immunoblot assay on supernatants and cell-associated proteins with Hcp6 antisera. Figure 3 shows that the Hcp6 antisera reacted with recombinant Hcp6, a protein with a predicted molecular mass of 22 kDa. Recombinant Hcp6 protein contained an additional 30 amino acids relative to native Hcp6, which had a predicted molecular mass of 18 kDa. The Hcp6 antisera also reacted with two bands in the cell lysate of the wild type, but not with any bands in the cell lysate of the Δ*hcp6* mutant (Fig. 3). This result strongly suggests that the bands of ~17 kDa and ~12 kDa were native Hcp6. It seemed unlikely that the 12-kDa protein was a proteolytic derivative of the 17-kDa protein, because no peptides of 6 kDa or smaller were detected in the immunoblot assays. A detailed analysis of the *hcp6* gene revealed an internal ATG codon, encoding methionine at position 59 in the native protein, which would result in a 12-kDa protein if translation initiated at this point. A potential ribosome binding site was also present immediately upstream of this putative alternative start codon. Surprisingly, there was no reactivity with either the 17-kDa or the 12-kDa protein in the wild-type supernatant. The data suggest that Hcp6 is produced *in vitro*, but that it is not exported to the extracellular milieu under the conditions tested. Intracellular Hcp6 in *B. pseudomallei* consists of two derivatives; one appears to be full-length Hcp6 and the other is likely a smaller derivative lacking the first 58 amino acids as the result of an alternative start codon.

**VirAG activates T6SS-1 transcription and Hcp1 export.** In a previous study, we found that the *B. mallei* ATCC 23344 *virAG* regulatory genes activated the transcription of T6SS-1 when expressed in *trans* from a broad-host-range vector (28). The *B. pseudomallei* K96243 VirA (BPSS1495) and VirG (BPSS1494) proteins are ~99% identical to the *B. mallei* ATCC 23344 VirA and VirG proteins, and we predicted that they would also activate T6SS-1 transcription in *B. pseudomallei*. We used SOLiD RNA sequencing technology to assess T6SS-1 transcript levels in *B. pseudomallei* AI harboring pBHR2 and pBHR2-*virAG*.

RPKM values for *B. pseudomallei* AI(pBHR2) and AI(pBHR2-*virAG*) were derived from three biological replicates in LB broth, with average QVs of 22.1 and 22.2, respectively. As expected, the genes encoding *virA* (BPSS1495) and

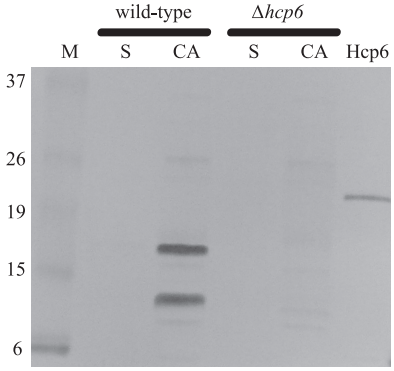


FIG. 3. Immunoblot analysis of *B. pseudomallei* Hcp6 production and export. *B. pseudomallei* wild-type and Δ*hcp6* cells were grown to logarithmic phase in LB, and the supernatant proteins (S) and cell-associated proteins (CA) were separated by SDS-PAGE, transferred to a polyvinylidenen difluoride membrane, and reacted with mouse polyclonal anti-Hcp6 sera. The relative migrations of molecular mass protein standards (M; in kDa) are indicated on the left. Purified recombinant Hcp6 served as a positive control for the experiment.

TABLE 5. *virAG* upregulates the *B. pseudomallei* T6SS-1 gene cluster and flanking genes

| Locus tag (gene) | Mean RPKM[a] | |
|---|---|---|
| | AI(pBHR2) | AI(pBHR2-*virAG*)[b] |
| BPSS1493 | 0.7 | 5.8 |
| BPSS1494 (*virG*) | 0.3 | 99.0 |
| BPSS1495 (*virA*) | 0.03 | 6.6 |
| BPSS1496 | 0.0 | 47.1 |
| BPSS1497 | 0.7 | 116 |
| BPSS1498 (*hcp1*) | 1.4 | 728 |
| BPSS1499 | 0.03 | 51.1 |
| BPSS1500 | 0.01 | 49.3 |
| BPSS1501 | 0.0 | 36.7 |
| BPSS1502 (*clpV1*) | 0.01 | 13.3 |
| BPSS1503 (*vgrG1*) | 0.06 | 18.8 |
| BPSS1504 | 0.01 | 3.3 |
| BPSS1505 | 0.01 | 3.1 |
| BPSS1506 | 0.0 | 2.1 |
| BPSS1507 | 0.0 | 21.2 |
| BPSS1508 | 0.0 | 5.8 |
| BPSS1509 | 0.0 | 8.9 |
| BPSS1510 | 0.0 | 8.0 |
| BPSS1511 (*icmF1*) | 0.01 | 7.4 |
| BPSS1512 (*tssM*) | 0.9 | 13.2 |
| BPSS1513 | 0.4 | 7.9 |
| BPSS1514 (*folE*) | 27.9 | 80.7 |
| BPSS1515 | 2.9 | 16.7 |

[a] Values are the mean RPKM for each gene from three biological replicates.
[b] *P* values were <0.001 for all comparisons [AI(pBHR2) versus AI(pBHR2-*virAG*)].

*virG* (BPSS1494) were expressed more highly in AI(pBHR2-*virAG*) than in AI(pBHR2) (Table 5). The mean RPKM values for *virA* and *virG* were 6.6 and 99.0, respectively, in AI(pBHR2-*virAG*), compared with values of 0.03 and 0.3 in AI(pBHR2). Overexpression of *virAG* had a dramatic impact on expression of genes in T6SS-1 (BPSS1496 to BPSS1511). Expression for each gene in T6SS-1 yielded significant differences in expression when compared directly between AI(pBHR2) and AI(pBHR2-*virAG*) (Table 5). The mean RPKM expression values for the T6SS-1 genes were 1.5 and 58.4 for AI(pBHR2) and AI(pBHR2-*virAG*), respectively (Table 5). Moreover, expression as a ratio to *narK* also yielded a statistically significant difference for each gene (data not shown). *B. pseudomallei hcp1* had the highest degree of upregulation by *virAG* in *trans*, increasing from an average RPKM of 1.4 in AI(pBHR2) to 728 in AI(pBHR2-*virAG*) (Table 5). Several genes flanking the T6SS-1 gene cluster were also transcribed at higher levels in the presence of *virAG*, including the gene encoding TssM deubiquitinase (30, 33). While all of the genes in the T6SS-1 cluster appear to be organized into an operon, it is unclear if there are intergenic promoters and/or transcriptional terminators that cannot be identified by sequence analysis alone. The presence of such intergenic elements may explain why not all *virAG*-activated genes in the T6SS-1 gene cluster display the same level of mean RPKM (Table 5). We concluded from these results that *virAG* activated the transcription of T6SS-1 when overexpressed in *trans*. Overexpression of *virAG* did not result in an increase in the transcription of T6SS-2, T6SS-3, T6SS-4, T6SS-5, or T6SS-6 (data not shown), and the regulators involved in the expression of these gene clusters are currently unknown.

We next determined if Hcp1 was produced and exported to the extracellular milieu in a VirAG-dependent manner. Figure 4A shows that Hcp1 was present in the supernatant of the wild-type strain, but only when *virAG* was overexpressed in *trans*. This demonstrated that VirAG transcriptional activation of T6SS-1 resulted in the export of Hcp1, which is a hallmark of a functional T6SS. As expected, Hcp1 was absent from the supernatant of the Δ*hcp1* mutant (Fig. 4A). To our knowledge, this is the first demonstration that the *B. pseudomallei* T6SS-1 encodes a functional secretion apparatus.

**VgrG1 N-terminal and C-terminal domains are required for optimal Hcp1 export.** Hcp and VgrG (valine-glycine repeat protein G) are encoded by most bacterial T6SS gene clusters, and they structurally resemble the tail and syringe of a bacteriophage tail, respectively (4, 26). Both are surface associated and mutually dependent on each other for export. While some VgrG proteins contain only a tail spike domain, the so-called "evolved VgrG" proteins contain C-terminal extensions with

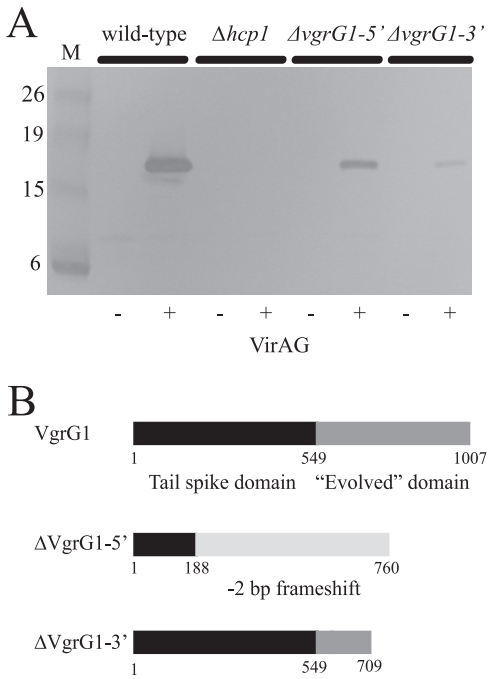


FIG. 4. Immunoblot analysis of *B. pseudomallei* Hcp1 export. (A) *B. pseudomallei* strains were grown to logarithmic phase in LB, and the supernatant proteins were separated by SDS-PAGE, transferred to a polyvinylidene difluoride membrane, and reacted with mouse polyclonal anti-Hcp1 sera. The *Burkholderia* strains used, AI (wild type), DDS1498 (Δ*hcp1*), DDS1503-1 (Δ*vgrG-5′*), and DDS1503-2 (Δ*vgrG1-3′*), all harbored pBHR2 (VirAG$^-$) or pBHR2-*virAG* (VirAG$^+$). The relative migrations of molecular mass protein standards (lane M; in kDa) are indicated on the left. (B) Schematic representation of native VgrG1 and VgrG1 derivatives generated by the Δ*vgrG-5′* and Δ*vgrG-3′* mutations. The proteins are represented as rectangles, and the domains are color coded black (tail spike domain) and dark gray ("evolved VgrG" domain). Light gray coloring represents amino acids not present in native VgrG1 resulting from a −2-bp frameshift in the coding sequence of the *vgrG1* gene due to the Δ*vgrG1-3′* mutation. The numbers under the proteins represent the number of amino acids in each protein.

TABLE 6. T6SS-1 is required for virulence in the Syrian hamster model of infection

| Strain | T6SS targeted | No. of animals that succumbed/total no. infected with[a]: | | | |
|---|---|---|---|---|---|
| | | $10^0$ | $10^1$ | $10^2$ | $10^3$ |
| K96243 | None | 5/5 | 5/5 | 5/5 | ND |
| Δ*hcp1* mutant | T6SS-1 | 0/5 | 0/5 | 0/5 | 0/5 |
| Δ*hcp1*/*hcp1*$^+$ mutant | T6SS-1 | 4/5 | 5/5 | 5/5 | ND |
| Δ*hcp2* mutant | T6SS-2 | 4/5 | 5/5 | 5/5 | ND |
| Δ*hcp3* mutant | T6SS-3 | 5/5 | 5/5 | 5/5 | ND |
| Δ*hcp4* mutant | T6SS-4 | 5/5 | 5/5 | 5/5 | ND |
| Δ*hcp5* mutant | T6SS-5 | 5/5 | 5/5 | 5/5 | ND |
| Δ*hcp6* mutant | T6SS-6 | 4/5 | 4/5 | 5/5 | ND |
| Δ*vgrG1-5′* mutant | T6SS-1 | 1/5 | 1/5 | 4/5 | ND |
| Δ*vgrG1-5′*/*vgrG1*$^+$ mutant | T6SS-1 | 2/5 | 5/5 | 5/5 | ND |
| Δ*vgrG1-3′* mutant | T6SS-1 | 0/5 | 0/5 | 0/5 | ND |
| Δ*vgrG1-3′*/*vgrG1*$^+$ mutant | T6SS-1 | 3/5 | 5/5 | 5/5 | ND |

[a] Groups of five female Syrian hamsters were infected i.p. with a range of $10^0$ to $10^3$ CFU for each strain examined. Mortality was recorded daily for 14 days. ND, not determined.

putative effector functions unrelated to Hcp export (26). *B. pseudomallei* K96243 VgrG1 (BPSS1503) is an "evolved VgrG" protein with an N-terminal tail spike domain and a C-terminal domain containing no significant similarity to any known proteins (Fig. 4B). In an attempt to identify a function for these distinct VgrG1 domains, we constructed 5′ and 3′ *vgrG1* deletion mutations and examined their effects on Hcp1 transport. The 5′ mutation (Δ*vgrG1-5′*) had only a moderate effect on Hcp1 export (Fig. 4A), which was unexpected, as the mutation resulted in a protein containing only the first 188 amino acids of the conserved tail spike domain of VgrG1 (Fig. 4B). The remainder of this 760-amino-acid protein contained amino acids not present in the native protein, due to a −2-bp frameshift mutation induced by the Δ*vgrG1-5′* deletion. This suggests that the first 188 amino acids of the 1,007-amino-acid VgrG1 protein are sufficient for Hcp1 export, although noticeably less Hcp1 was present in the Δ*vgrG1-5′* supernatant than in the wild-type supernatant (Fig. 4).

In comparison, the 3′ mutation (Δ*vgrG1-3′*) had a very pronounced effect on Hcp1 export (Fig. 4A). This in-frame mutation resulted in a protein lacking amino acids 589 to 886 of the "evolved" C-terminal domain of VgrG1, which was predicted to play no role in Hcp1 export. It was surprising that this mutation had such a pronounced effect on Hcp1 export, as the entire N-terminal tail spike domain is present in this protein. Taken together, the results suggested that the conserved N-terminal and the novel C-terminal domains of VgrG1 are both required for optimal Hcp1 export. This may represent the first instance where an evolved VgrG domain plays a role in the export of Hcp, although we cannot rule out the possibility that the Δ*vgrG1-3′* mutation results in a protein with a conformational abnormality that alters protein stability or prohibits normal functioning of the N-terminal tail spike domain.

**T6SS-1 is a major virulence factor in the Syrian hamster model of melioidosis.** The Δ*hcp* mutants and the Δ*vgrG1* mutants were examined for their relative virulence in the hamster model of infection. Syrian hamsters are exquisitely sensitive to infection with *B. pseudomallei* (10), and the $LD_{50}$ for K96243 was <10 CFU (Table 6). The $LD_{50}$ for the Δ*hcp1* mutant, on the other hand, was $>10^3$ CFU. This represents at least a 1,000-fold difference in virulence between the wild-type strain and the Δ*hcp1* mutant. The *hcp1* deletion mutant was complemented when *hcp1* was supplied in *trans* on a broad-host-range plasmid (Δ*hcp1*/*hcp1*$^+$), demonstrating that this mutation is not polar and that T6SS-1 is critical for virulence (Table 6). The $LD_{50}$ values for the Δ*hcp2* through Δ*hcp6* mutants were indistinguishable from that of the wild type, suggesting that T6SS-2, T6SS-3, T6SS-4, T6SS-5, and T6SS-6 are not required for virulence in this animal model of infection (Table 6).

We next examined the relative virulence of the Δ*vgrG1-5′* and Δ*vgrG1-3′* mutants and found that they exhibited $LD_{50}$ values of 102 and >450 CFU, respectively (Table 6). The reduced virulence of these strains relative to the wild type further supports the notion that T6SS-1 is an important *B. pseudomallei* virulence determinant. The results were intriguing, because the virulence phenotype of these mutants resembled their Hcp1 export phenotype (Table 6 and Fig. 4A). In fact, there appears to be an overall correlation between Hcp1 export and virulence (wild type > Δ*vgrG1-5′* mutant > Δ*vgrG1-3′*/Δ*hcp1* mutant). Both Δ*vgrG1* mutants were complemented when *vgrG1* was supplied in *trans* on a broad-host-range plasmid (Table 6), demonstrating that the Δ*vgrG1* mutations did not have polar effects on downstream genes. Taken together, the results demonstrate that T6SS-1 is a major virulence determinant in *B. pseudomallei* and that the other T6SS gene clusters may be involved in some other aspect of *B. pseudomallei*'s saprophytic lifestyle.

**Comparative histopathology of hamsters infected with wild-type and Δ*hcp1* strains.** At 48 h postinfection, histopathology studies were conducted on hamsters infected with either the wild type or the Δ*hcp1* mutant. The animals infected with the wild-type strain (~8 CFU) were moribund at the time of euthanasia, but animals infected with the Δ*hcp1* mutant (~630 CFU) appeared healthy. The organs from the infected animals were extracted, fixed, and stained with H&E for histopathological analysis. Numerous foci of pyogranulomatous inflammatory cell infiltrates were identified in the liver of the hamster infected with the wild type, with corresponding degeneration and loss of hepatocytes (Fig. 5A and B). In these lesions, many of the inflammatory cells were necrotic (Fig. 5B). Bacteria, although not numerous, were evident in macrophages in these lesions. In the spleens there were also numerous foci of pyogranulomatous inflammatory cell infiltrates with necrosis of many of the inflammatory cells. As in the liver, bacilli were evident in small numbers within macrophages. Mesenteric lymph nodes had similar inflammatory cell infiltrates with scant bacilli. Finally, there were scattered foci of granulomatous inflammatory cell infiltrates in the marrow of the maxilla, but no bacilli were evident in these lesions (data not shown).

Although the hamsters infected with the Δ*hcp1* mutant appeared healthy 48 h postinfection, there was clear histological evidence that the hamsters had been infected. The livers had numerous foci of granulomatous (i.e., mostly macrophages) to pyogranulomatous (i.e., roughly equal numbers of macrophages and neutrophils) inflammatory cell infiltrates (Fig. 5C and D). Unlike hamsters infected with the wild-type strain, there were no bacilli discernible in the liver infiltrates and there was no evidence of necrosis (Fig. 5D). This result suggests a more quiescent and less aggressive infection, a histo-

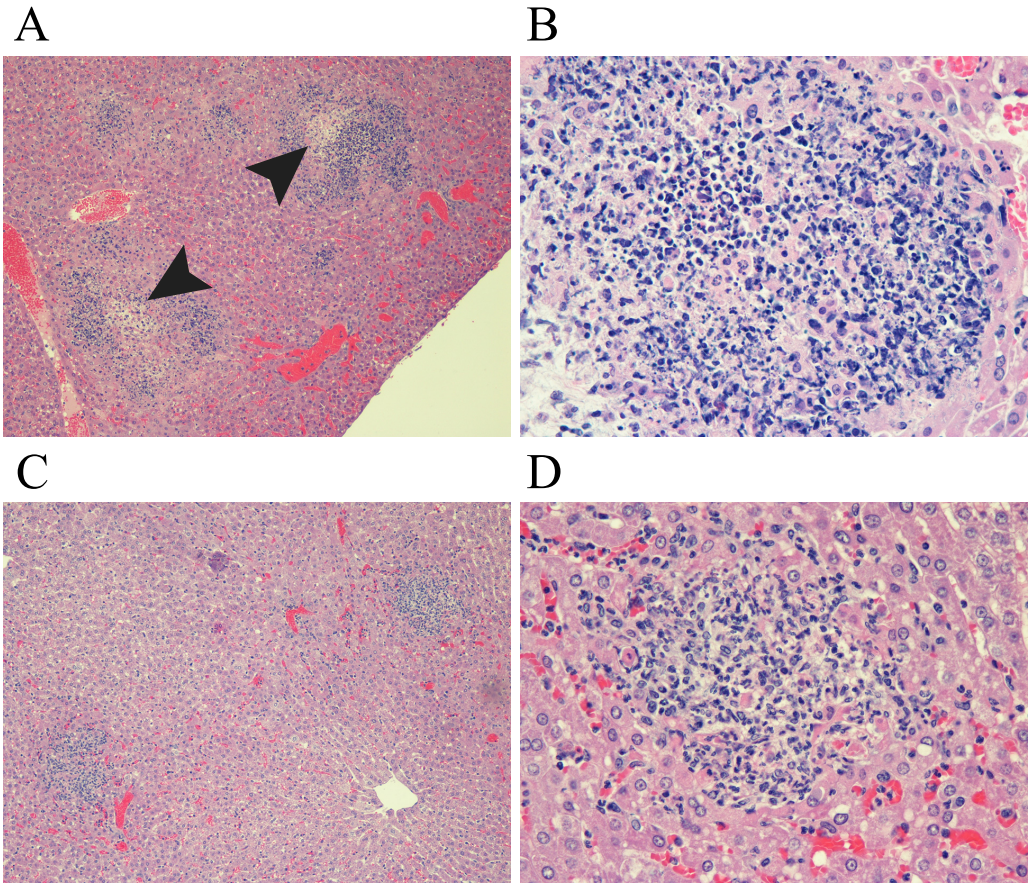


FIG. 5. Hepatic inflammatory cell infiltrates 2 days after infection with *B. pseudomallei*. Fixed and sectioned liver tissues from hamsters infected i.p. with wild-type (A and B) and Δ*hcp1* (C and D) strains were stained with H&E and viewed at 10× (A and C) and 40× (B and D) magnification. The livers from hamsters infected with the wild type contained areas with damaged hepatocytes (arrowheads) and necrotic infiltrates of neutrophils and macrophages. Necrosis and damaged hepatocytes were not observed in the hepatic inflammatory infiltrates from hamsters infected with the Δ*hcp1* mutant, suggesting a role for T6SS-1 in these processes.

logical indication that the Δ*hcp1* mutant is not as pathogenic as the wild type. Similarly, spleens from Δ*hcp1* mutant-infected hamsters had numerous foci of similar infiltrates with no bacilli evident in these lesions. In contrast to the wild-type-infected hamsters, the mesenteric lymph nodes and bone marrow were not affected in the Δ*hcp1* mutant-infected hamsters (data not shown).

Taken together, the most notable histopathological differences between these two groups of hamsters were that inflammatory infiltrates in the animals infected with the Δ*hcp1* mutant were more quiescent and had the character of resolving lesions, whereas the infiltrates in the animals infected with the wild type were much more active and aggressive. In addition, intracellular bacilli were identified in wild-type lesions, whereas no intracellular organisms were observed in the lesions of Δ*hcp1* mutant-infected animals.

**T6SS-1 is required for multinucleated giant cell formation, growth, and cytotoxicity in RAW 264.7 macrophages.** We recently demonstrated that the *B. mallei* T6SS-1 was important for actin polymerization, MNGC formation, and growth in phagocytic cells (8), and we wanted to determine if this was also true for the T6SS-1 of *B. pseudomallei*. RAW 264.7 monolayers were infected with GFP-expressing *B. pseudomallei* strains, and at 12 and 18 h postinfection they were stained with Alexa Fluor 568 phalloidin and DRAQ5 and fluorescent images were captured. Figure 6 shows that by 12 h postinfection the wild type had formed MNGC (Fig. 6A) but that the Δ*hcp1* mutant had not (Fig. 6B). In fact, not a single RAW 264.7 MNGC was observed at 12 or 18 h postinfection with the Δ*hcp1* mutant. Both *B. pseudomallei* strains were visible within the macrophages, so a lack of uptake of the Δ*hcp1* mutant was not responsible for this phenotype (Fig. 6A, B, and E). Interestingly, and in contrast to what was seen with a *B. mallei* T6SS-1 mutant (8), there was a less obvious difference in the extent of actin polymerization between the *B. pseudomallei* wild-type and Δ*hcp1* strains. There was extensive damage to the wild-type-infected macrophage monolayer by 18 h with a corresponding decrease in the amount of GFP-labeled bacteria present in any given field (Fig. 6C). In comparison, the Δ*hcp1* mutant-infected macrophages were largely intact and filled with GFP-labeled bacteria at 18 h postinfection (Fig. 6D).

We next conducted modified Km protection assays to determine uptake, survival, and replication of the wild type and Δ*hcp1* mutant inside macrophages. RAW264.7 cells were infected with an MOI of 1, and by 3 h postinfection similar numbers of intracellular wild-type and Δ*hcp1* bacteria were

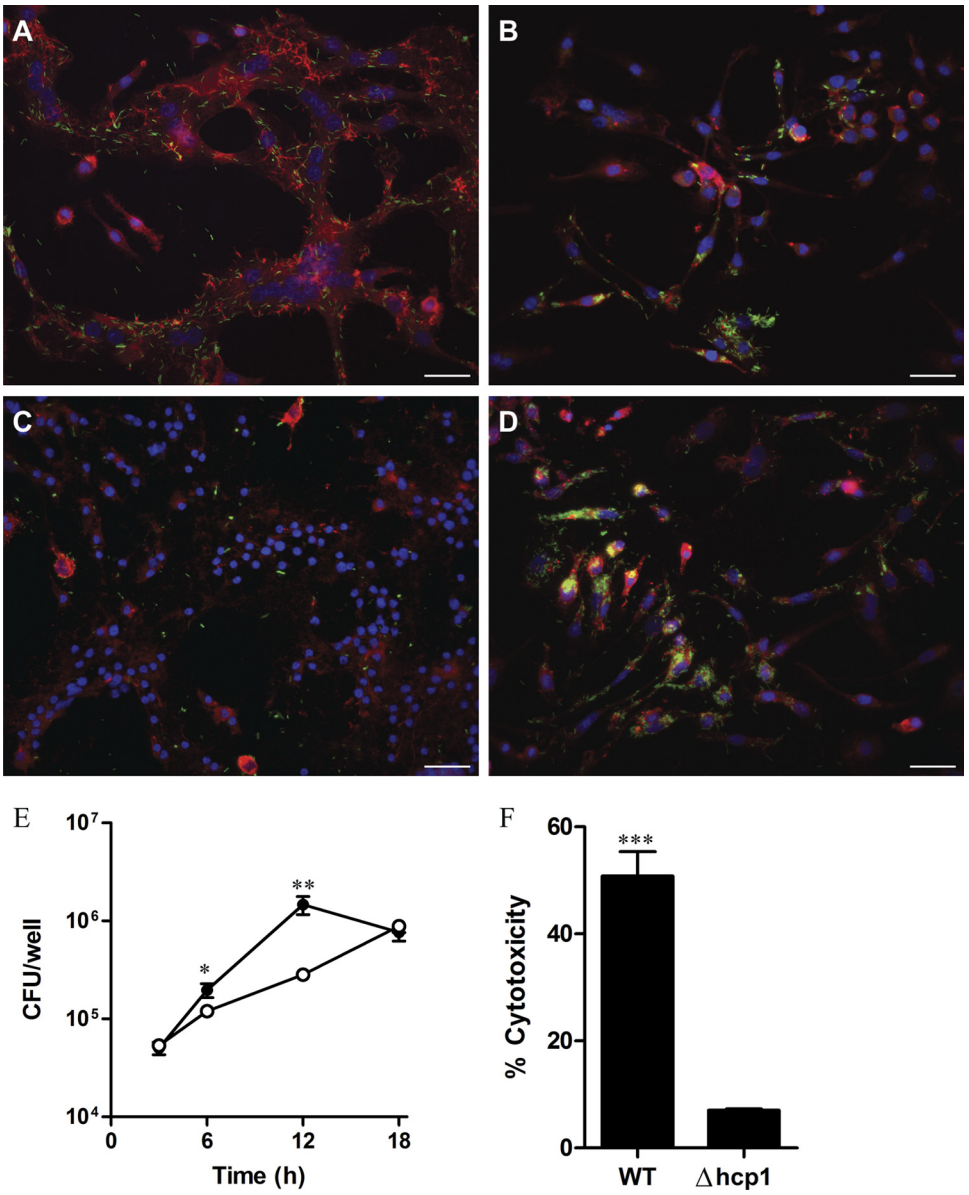


FIG. 6. The *B. pseudomallei* Δ*hcp1* mutant exhibits MNGC, growth, and cytotoxicity defects in RAW 264.7 cells. Monolayers infected with *B. pseudomallei* wild type (A and C) or Δ*hcp1* (B and D) cells harboring pBHR1-TG were fixed at 12 h (A and B) and 18 h (C and D) postinfection, stained, and examined by fluorescence microscopy. Bacteria expressing GFP are shown in green, host cell actin stained with Alexa 568 phalloidin is shown in red, and nuclei stained with DRAQ5 are shown in blue. Micrographs are representative of at least three independent experiments. Bars, 20 μm. (E) Monolayers infected with *B. pseudomallei* wild type (closed circles) or the Δ*hcp1* mutant (open circles) and uptake and survival were quantitated by utilizing a modified Km protection assay at 3, 6, 12, and 18 h postinfection. All assays were conducted on at least two separate occasions. The error bars represent standard deviations. *, $P < 0.05$; **, $P < 0.01$. (F) Filter-sterilized *B. pseudomallei*-infected RAW 264.7 cell supernatants were assayed for LDH release at 18 h postinfection. The error bars represent standard deviations. ***, $P < 0.001$; WT, wild type.

present (Fig. 6E), suggesting no differences in uptake. The number of intracellular wild-type bacteria at the 12-h time point was ~10-fold higher than that of the Δ*hcp1* mutant (Fig. 6E). However, the Δ*hcp1* mutant appeared to demonstrate a delayed growth phenotype, as it continued to increase in number to the 18-h time point (Fig. 6E). The number of wild-type bacteria started to decrease by 18 h and was consistent with the fluorescence microscopy results described above (Fig. 6C and D). This phenomenon is likely due to wild-type bacteria being killed by Km in the extracellular medium rather than by RAW 264.7 cells directly. These results clearly demonstrate that the T6SS-1 mutant exhibits a significant delay in intracellular growth relative to the wild type, which is inconsistent with the results from a previously published study (29).

It seemed likely from the above experiments that the wild type was killing the macrophage monolayers by 18 h but that the Δ*hcp1* mutant was not (Fig. 6C, D, and E). Thus, we examined the relative cytotoxicity of the wild-type and Δ*hcp1*

strains at this time point by examining the release of LDH from the infected monolayers. Approximately 50% of the wild-type-infected macrophages were lysed at 18 h, while <10% of Δ*hcp1* mutant-infected macrophages were lysed (Fig. 6F). The significantly lower cytotoxicity of the Δ*hcp1* mutant correlated well with the fluorescence microscopy experiments (Fig. 6C and D) and the Km protection assays (Fig. 6E) described above. The results suggest that the *B. pseudomallei* T6SS-1 plays important roles in MNGC formation, intracellular growth, and cytotoxicity in macrophages *in vitro*.

## DISCUSSION

Here, we provide the first comprehensive description of T6SSs in *B. pseudomallei*, an organism that harbors more T6SS gene clusters than any other fully sequenced microbe (5). We found T6SS-1 to be a major virulence determinant that plays an important role in the intracellular lifestyle of this pathogen. The T6SS-1 Hcp1 protein was recognized by sera from melioidosis patients, demonstrating that this protein is immunogenic and is produced *in vivo* (Fig. 2B). The *B. mallei* Hcp1 protein was also recognized by sera from animals and a human patient with glanders (28), suggesting that Hcp1 might be a good *Burkholderia* vaccine candidate. A recent study by Whitlock et al. (39) demonstrated that 75% of mice vaccinated with recombinant Hcp1 from *B. mallei* were protected from a subsequent intranasal challenge with wild-type bacteria. However, the spleens from all surviving Hcp1-vaccinated animals were colonized and sterilizing immunity was not attained. We tested recombinant *B. pseudomallei* Hcp1 as a vaccine candidate in a murine model of melioidosis and found that it provided inadequate protection against an otherwise-lethal *B. pseudomallei* challenge (Table 3). Similarly, recombinant Hcp2 through -6 proteins provided poor protection and/or a lack of sterilizing immunity against a lethal bacterial challenge. While the results indicate that *B. pseudomallei* Hcp proteins are unlikely to serve as vaccine candidates, it is possible that Hcp1 could be used as a serological reagent for the diagnosis of melioidosis in humans. Further studies are warranted to study the percentage of melioidosis serum samples that react with Hcp1 and to determine if a positive result is indicative of an active or a chronic infection.

In many bacteria, the expression of T6SS gene clusters is tightly regulated at the transcriptional level, so that T6SSs are produced only when appropriate environmental cues are present (2). We performed expression profiling *in vitro* and found that five of the six T6SS gene clusters were expressed poorly when *B. pseudomallei* was grown in LB broth (Table 4). Only the T6SS-6 gene cluster was constitutively expressed *in vitro*, suggesting that T6SS clusters 1 through 5 do not function in this environment. As expected, Hcp1 through -5 proteins were not produced or exported when *B. pseudomallei* was grown in LB broth. *B. pseudomallei* Hcp6 was produced *in vitro*, but it was not exported. This was a surprising result, because Hcp export is a hallmark of a functional T6SS (4). Previous studies have shown that Hcp is dependent upon VgrG for export outside the cell, and vice versa (25, 42). The *B. pseudomallei* T6SS-6 gene cluster does not encode a VgrG protein (28, 29), and we hypothesize that Hcp6 cannot be exported without a corresponding VgrG protein. VgrG proteins are an essential component of the T6SS apparatus, as they form the cell-puncturing device for delivering effector molecules into target cells. Thus, it is currently unclear how the *B. pseudomallei* T6SS-6 functions without an encoded VgrG protein. It is possible that it "borrows" one of the other VgrG proteins encoded elsewhere in the genome, but further work will be required to fully understand the mechanism of action of T6SS-6.

A two-component regulatory system, termed VirAG, is encoded immediately upstream of the *B. pseudomallei* T6SS-1 gene cluster. In *B. mallei*, overexpression of the *virAG* genes in *trans* resulted in the expression of the T6SS-1 gene cluster and led to the production and export of Hcp1 (28). We demonstrated here that the *B. pseudomallei hcp1* gene was induced over 500-fold with *virAG* in *trans* (Table 5) and that Hcp1 was produced and exported in a VirAG-dependent manner (Fig. 4). The environmental cue(s) sensed by VirA is currently unknown, but a previous study revealed that the *B. pseudomallei* T6SS-1 cluster was specifically induced inside macrophages (29). Similarly, expression of the *B. mallei* T6SS-1 gene cluster occurs within the macrophage prior to escape from the phagosome (8). VirAG may sense specific conditions within phagocytic vacuoles, and in response, activate transcription of the T6SS-1 genes. However, it is currently unknown if transcriptional activation of the T6SS-1 genes by VirAG is direct or indirect. While transcriptional regulation of the *B. pseudomallei* T6SS-1 gene cluster is complex, we know that it is "turned on" immediately after the type III secretion system gene cluster 3 (T3SS-3) and that BspR, BprP, BsaN, VirAG, and BprC all influence its expression (28).

We hypothesize that once activated, the T6SS-1 translocates an effector molecule(s) across the phagosomal membrane directly into the cytosol in preparation for arrival of the bacterium to this niche. In support of this notion, we found that the Δ*hcp1* mutant exhibited a significant delay in intracellular growth in RAW 264.7 macrophages. The numbers of intracellular wild-type and Δ*hcp1* cells were similar at 3 h postinfection, but by 12 h there were ~10-fold fewer Δ*hcp1* cells (Fig. 6E). By 18 h postinfection, the numbers of intracellular wild-type and Δ*hcp1* cells were similar, as Δ*hcp1* cells continued to replicate intracellularly while the wild type was released into the antibiotic-containing extracellular medium and killed. There appears to be a threshold of intracellular bacteria that RAW 264.7 cells can harbor before lysis occurs (Fig. 6A and C), and this number occurs at 12 h postinfection for the wild type and at >18 h for the Δ*hcp1* mutant. This is consistent with the macrophage cytotoxicity data at 18 h postinfection for the wild type (50% cytotoxicity) and the Δ*hcp1* mutant (<10% cytotoxicity) (Fig. 6F). The results indicate that T6SS-1 is important for efficient intracellular growth inside macrophages, which is especially noticeable between 6 and 12 h postinfection (Fig. 6E). Shalom et al. did not find an intracellular growth defect with their *B. pseudomallei* T6SS-1 mutant; however, they only determined CFU counts at 4 and 19 h postinfection (29). We propose that if they had performed counts at more time points between 4 and 19 h, they would have noticed the growth defect that we observed with the Δ*hcp1* mutant. Another *B. mallei* T6SS-1 mutant also exhibited an intracellular growth defect, which further supports the notion that T6SS-1 is important for this phenotype (8).

Another important observation we made with the Δ*hcp1*

mutant was that it was unable to form MNGC in RAW 264.7 cell monolayers (Fig. 6B and D). The mutant replicated to high numbers in the cytosol by 18 h postinfection (Fig. 6D), but no fusion with adjacent cells occurred. Cell-to-cell fusion and the formation of MNGC is a hallmark of *B. pseudomallei* infection in phagocytic and nonphagocytic cell lines (3, 15, 19), and MNGC have been observed in cases of human melioidosis (41), suggesting a role in pathogenicity. MNGC are predicted to be important for evasion of host immune responses and persistence of *B. pseudomallei* within the host (11). The formation of MNGC does not occur if bacterial protein synthesis is inhibited after *B. pseudomallei* is internalized in RAW 264.7 cells (35), suggesting that a bacterial factor needs to be actively synthesized intracellularly for MNGC to form. We propose that a T6SS-1 effector mediates MNGC formation by activating molecular machinery involved in macrophage fusion (16). Furthermore, we hypothesize that the nutrients provided when an uninfected macrophage fuses with a *B. pseudomallei*-infected MNGC are responsible for the observed growth advantage of the wild type over the Δ*hcp1* mutant. More research will be necessary to identify the putative T6SS-1 effector(s) involved in MNGC formation and intracellular growth of *B. pseudomallei*.

We demonstrated in this study that T6SS-1 is a major virulence determinant in the hamster model of melioidosis (Table 6). In fact, the Δ*hcp1* mutant exhibited one of the highest $LD_{50}$ values ever described in this animal model ($>10^3$ CFU), despite the fact that we didn't determine the $LD_{50}$ until 14 days after challenge. Two *vgrG1* deletion mutants were also attenuated in hamsters, and their level of attenuation correlated with the amount of Hcp1 that they exported *in vitro*, suggesting a link between virulence and the relative function of T6SS-1 (Fig. 4 and Table 6). The livers, spleens, and mesenteric lymph nodes of hamsters infected with the Δ*hcp1* mutant displayed no necrosis of inflammatory cell infiltrates (Fig. 5), suggesting that the inflammatory infiltrates were much less aggressive than what was found in animals infected with the wild type. In addition, no bacteria could be identified inside the macrophages present in these inflammatory infiltrates. While MNGC have been identified in human cases of melioidosis (41), no MNGC were observed in any of the affected organs of hamsters challenged with the wild type. This result was surprising, given the fact that there appeared to be a correlation between virulence and MNGC formation with wild-type and Δ*hcp1* bacteria (Table 6 and Fig. 6). The hamster represents an acute model of melioidosis, and perhaps the rapidity of death limits its usefulness for identifying MNGC in tissues. Pilatz et al. (24) demonstrated that a T6SS-1 transposon mutant was attenuated in BALB/c mice, but they did not perform a histological analysis of the organs of the infected animals. It is possible that MNGC formation *in vivo* might be more easily studied in a chronic model of melioidosis. At the moment, the relationship between the formation of MNGC by *B. pseudomallei* and pathogenesis in melioidosis is unclear.

## ACKNOWLEDGMENTS

D.D. conducted research on this project at Dstl Porton Down for 9 months as part of The Technical Cooperation Program (TTCP). The sabbatical leave and research was funded by the Defense Threat Reduction Agency (DTRA)/Joint Science and Technology Office for Chemical and Biological Defense (JSTO-CBD) (proposal number 2.10018_06_RD_B) and by the UK Ministry of Defense. This project also received support from DTRA/JSTO-CBD proposal number CBS.MEDBIO.02.10.RD.034 (to D.D.) and agreement no. HSHQDC-07-C-00020 awarded by the U.S. Department of Homeland Security for the management and operation of the National Biodefense Analysis and Countermeasures Center (NBACC).

We thank Nicki Walker, Lynda Miller, Steve Tobery, and Anthony Bassett for advice and technical assistance.

## REFERENCES

1. **Ashdown, L. R.** 1979. Identification of *Pseudomonas pseudomallei* in the clinical laboratory. J. Clin. Pathol. **32:**500–504.
2. **Bernard, C. S., Y. R. Brunet, E. Gueguen, and E. Cascales.** 2010. Nooks and crannies in type VI secretion regulation. J. Bacteriol. **192:**3850–3860.
3. **Boddey, J. A., et al.** 2007. The bacterial gene *lfpA* influences the potent induction of calcitonin receptor and osteoclast-related genes in *Burkholderia pseudomallei*-induced TRAP-positive multinucleated giant cells. Cell. Microbiol. **9:**514–531.
4. **Bönemann, G., A. Pietrosiuk, and A. Mogk.** 2010. Tubules and donuts: a type VI secretion story. Mol. Microbiol. **76:**815–821.
5. **Boyer, F., G. Fichant, J. Berthod, Y. Vandenbrouck, and I. Attree.** 2009. Dissecting the bacterial type VI secretion system by a genome wide in silico analysis: what can be learned from available microbial genomic resources? BMC Genomics **10:**104.
6. **Brett, P. J., M. N. Burtnick, H. Su, V. Nair, and F. C. Gherardini.** 2008. iNOS activity is critical for the clearance of *Burkholderia mallei* from infected RAW 264.7 murine macrophages. Cell. Microbiol. **10:**487–498.
7. **Burtnick, M. N., et al.** 2008. *Burkholderia pseudomallei* type III secretion system mutants exhibit delayed vacuolar escape phenotypes in RAW 264.7 murine macrophages. Infect. Immun. **76:**2991–3000.
8. **Burtnick, M. N., D. DeShazer, V. Nair, F. C. Gherardini, and P. J. Brett.** 2010. *Burkholderia mallei* cluster 1 type VI secretion mutants exhibit growth and actin polymerization defects in RAW 264.7 murine macrophages. Infect. Immun. **78:**88–99.
9. **DeShazer, D., P. J. Brett, R. Carlyon, and D. E. Woods.** 1997. Mutagenesis of *Burkholderia pseudomallei* with Tn*5*-OT182: isolation of motility mutants and molecular characterization of the flagellin structural gene. J. Bacteriol. **179:**2116–2125.
10. **DeShazer, D., and D. E. Woods.** 1999. Animal models of melioidosis, p. 199–203. *In* O. Zak and M. Sande (ed.), Handbook of animal models of infection. Academic Press Ltd., London, England.
11. **Galyov, E. E., P. J. Brett, and D. DeShazer.** 2010. Molecular insights into *Burkholderia pseudomallei* and *Burkholderia mallei* pathogenesis. Annu. Rev. Microbiol. **64:**495–517.
12. **Gilad, J., I. Harary, T. Dushnitsky, D. Schwartz, and Y. Amsalem.** 2007. *Burkholderia mallei* and *Burkholderia pseudomallei* as bioterrorism agents: national aspects of emergency preparedness. Isr. Med. Assoc. J. **9:**499–503.
13. **Godoy, D., et al.** 2003. Multilocus sequence typing and evolutionary relationships among the causative agents of melioidosis and glanders, *Burkholderia pseudomallei* and *Burkholderia mallei*. J. Clin. Microbiol. **41:**2068–2079.
14. **Hamad, M. A., S. L. Zajdowicz, R. K. Holmes, and M. I. Voskuil.** 2009. An allelic exchange system for compliant genetic manipulation of the select agents *Burkholderia pseudomallei* and *Burkholderia mallei*. Gene **430:**123–131.
15. **Harley, V. S., D. A. B. Dance, B. S. Drasar, and G. Tovey.** 1998. Effects of *Burkholderia pseudomallei* and other *Burkholderia* species on eukarotic cells in tissue culture. Microbios **96:**71–93.
16. **Helming, L., and S. Gordon.** 2009. Molecular mediators of macrophage fusion. Trends Cell. Biol. **19:**514–522.
17. **Holden, M. T., et al.** 2004. Genomic plasticity of the causative agent of melioidosis, *Burkholderia pseudomallei*. Proc. Natl. Acad. Sci. U. S. A. **101:**14240–14245.
18. **Hood, R. D., et al.** 2010. A type VI secretion system of *Pseudomonas aeruginosa* targets a toxin to bacteria. Cell Host Microbe **7:**25–37.
19. **Kespichayawattana, W., S. Rattanachetkul, T. Wanun, P. Utaisincharoen, and S. Sirisinha.** 2000. *Burkholderia pseudomallei* induces cell fusion and actin-associated membrane protrusion: a possible mechanism for cell-to-cell spreading. Infect. Immun. **68:**5377–5384.
20. **Logue, C.-A., I. R. Peak, and I. R. Beacham.** 2009. Facile construction of unmarked deletion mutants in *Burkholderia pseudomallei* using *sacB* counter-selection in sucrose-resistant and sucrose-sensitive isolates. J. Microbiol. Methods **76:**320–323.
21. **Ma, A. T., S. McAuley, S. Pukatzki, and J. J. Mekalanos.** 2009. Translocation of a *Vibrio cholerae* type VI secretion effector requires bacterial endocytosis by host cells. Cell Host Microbe **5:**234–243.
22. **National Research Council.** 1996. Guide for the care and use of laboratory animals. National Academy Press, Washington, DC.
23. **Ngauy, V., Y. Lemeshev, L. Sadkowski, and G. Crawford.** 2005. Cutaneous melioidosis in a man who was taken as a prisoner of war by the Japanese during World War II. J. Clin. Microbiol. **43:**970–972.

24. **Pilatz, S., et al.** 2006. Identification of *Burkholderia pseudomallei* genes required for the intracellular life cycle and *in vivo* virulence. Infect. Immun. **74:**3576–3586.
25. **Pukatzki, S., A. T. Ma, A. T. Revel, D. Sturtevant, and J. J. Mekalanos.** 2007. Type VI secretion system translocates a phage tail spike-like protein into target cells where it cross-links actin. Proc. Natl. Acad. Sci. U. S. A. **104:** 15508–15513.
26. **Pukatzki, S., S. B. McAuley, and S. T. Miyata.** 2009. The type VI secretion system: translocation of effectors and effector-domains. Curr. Opin. Microbiol. **12:**11–17.
27. **Reed, L. J., and H. Muench.** 1938. A simple method of estimating fifty per cent endpoints. Am. J. Hyg. (Lond.) **27:**493–497.
28. **Schell, M. A., et al.** 2007. Type VI secretion is a major virulence determinant in *Burkholderia mallei*. Mol. Microbiol. **64:**1466–1485.
29. **Shalom, G., J. G. Shaw, and M. S. Thomas.** 2007. In vivo expression technology identifies a type VI secretion system locus in *Burkholderia pseudomallei* that is induced upon invasion of macrophages. Microbiology **153:**2689–2699.
30. **Shanks, J., et al.** 2009. *Burkholderia mallei tssM* encodes a putative deubiquitinase that is secreted and expressed inside infected RAW 264.7 murine macrophages. Infect. Immun. **77:**1636–1648.
31. **Simon, R., U. Priefer, and A. Puhler.** 1983. A broad host range mobilization system for *in vivo* genetic engineering: tranposon mutagenesis in gram negative bacteria. Biotechnology (NY) **1:**784–791.
32. **Sprague, L. D., and H. Neubauer.** 2004. Melioidosis in animals: a review on epizootiology, diagnosis and clinical presentation. J. Vet. Med. B Infect. Dis. Vet. Public Health **51:**305–320.
33. **Tan, K. S., et al.** 2010. Suppression of host innate immune response by *Burkholderia pseudomallei* through the virulence factor TssM. J. Immunol. **184:**5160–5171.
34. **Ulrich, R. L., K. Amemiya, D. M. Waag, C. J. Roy, and D. DeShazer.** 2005. Aerogenic vaccination with a *Burkholderia mallei* auxotroph protects against aerosol-initiated glanders in mice. Vaccine **23:**1986–1992.
35. **Utaisincharoen, P., S. Arjcharoen, K. Limposuwan, S. Tungpradabkul, and S. Sirisinha.** 2006. *Burkholderia pseudomallei* RpoS regulates multinucleated giant cell formation and inducible nitric oxide synthase expression in mouse macrophage cell line (RAW 264.7). Microb. Pathog. **40:**184–189.
36. **Vietri, N. J., and D. DeShazer.** 2007. Melioidosis, p. 147–166. *In* Z. F. Dembek (ed.), Medical aspects of biological warfare. Department of the Army, Office of The Surgeon General, Borden Institute, Washington, DC.
37. **Voskuhl, G. W., P. Cornea, M. S. Bronze, and R. A. Greenfield.** 2003. Other bacterial diseases as a potential consequence of bioterrorism: Q fever, brucellosis, glanders, and melioidosis. J. Okla. State Med. Assoc. **96:**214–217.
38. **Waag, D. M., and D. DeShazer.** 2004. Glanders: new insights into an old disease, p. 209–237. *In* L. E. Lindler, F. J. Lebeda, and G. W. Korch (ed.), Biological weapons defense: infectious diseases and counterbioterrorism. Humana Press Inc., Totowa, NJ.
39. **Whitlock, G. C., et al.** 2010. Protective response to subunit vaccination against intranasal *Burkholderia mallei* and *B. pseudomallei* challenge. Proc. Vaccinol. **2:**73–77.
40. **Wilson, K.** 1987. Preparation of genomic DNA from bacteria, p. 2.4.1–2.4.5. *In* F. M. Ausubel, R. Brent, R. E. Kingston, D. D. Moore, J. G. Seidman, J. A. Smith, and K. Struhl (ed.), Current protocols in molecular biology. John Wiley & Sons, New York, NY.
41. **Wong, K. T., S. D. Puthucheary, and J. Vadivelu.** 1995. The histopathology of human melioidosis. Histopathology **26:**51–55.
42. **Zheng, J., and K. Y. Leung.** 2007. Dissection of a type VI secretion system in *Edwardsiella tarda*. Mol. Microbiol. **66:**1192–1206.

*Editor:* J. B. Bliska